JOURNAL OF Applied Polymer SCIENCE

Ionic Conductivity, Dielectric Behavior, and HATR-FTIR Analysis onto Poly(methyl methacrylate)-Poly(vinyl chloride) Binary Solid Polymer Blend Electrolytes

S. Ramesh, Chiam-Wen Liew, K. Ramesh
Centre for Ionics University Malaya, Department of Physics, Faculty of Science, University of Malaya, 50603 Kuala Lumpur, Malaysia
Correspondence to: S. Ramesh (E-mail: rameshtsubra@gmail.com)

ABSTRACT: Solid polymer electrolytes comprising blends of poly(vinyl chloride) (PVC) and poly(methyl methacrylate) (PMMA) as host polymers and lithium bis(trifluoromethanesulfonyl) imide (LiTFSI) as dopant salt were prepared by solution-casting technique. The ionic conductivity and dielectric behavior were investigated by using AC-impedance spectroscopy in the temperature range of 298–353 K. The highest ionic conductivity of $(1.11 \pm 0.09) \times 10^{-6}$ S cm^{-1} is obtained at room temperature. The temperature dependence of ionic conductivity plots showed that these polymer blend electrolytes obey Arrhenius behavior. Conductivity–frequency dependence, dielectric relaxation, and dielectric moduli formalism were also further discussed. Apart from that, the structural characteristic of the polymer blend electrolytes was characterized by means of horizontal attenuated total reflectance–Fourier transform infrared (HATR–FTIR) spectroscopy. HATR–FTIR spectra divulged the interaction between PMMA, PVC, and LiTFSI. © 2012 Wiley Periodicals, Inc. J. Appl. Polym. Sci. 000: 000–000, 2012

KEYWORDS: PMMA; PVC; dielectric behavior; HATR-FTIR

Received 11 November 2010; accepted 21 February 2012; published online
DOI: 10.1002/app.37532

INTRODUCTION

Solid polymer electrolytes (SPEs) manifest wide range of applications in the technology field, ranging from small-scale production of commercial secondary lithium batteries (also known as the rechargeable batteries) to advanced high energy electrochemical devices, such as chemical sensors, fuel cells, electrochromic windows, supercapacitors, analog memory devices, and dye-sensitized solar cells (DSSCs). As for the commercial promises of lithium rechargeable batteries, there is a wide range of application, which ranges from portable electronic and personal communication devices such as laptop, mobile phone, MP3 player, PDA to hybrid electrical vehicle (EV), and start–light–ignition (SLI), which serves as traction power source for electricity.[1] SPEs are formed by doping a low lattice energy metal salt in polymer matrix, and the solution is thus dissolved by aprotic solvent. A force had been driven in the development of SPE because of its high automation potential for electrode application, high ambient temperature–ionic conductivity, wide operating temperature range, and low volatility as well as less probability for leaking noncorrosive medium.[2,3] In addition, the electrochemical, structural, thermal, photochemical, and chemical stability can be enhanced for SPEs in comparison with conventional liquid electrolyte.

Many approaches have been performed to increase ionic conductivity at ambient temperature, including polymer blending, cross-linking of two different types of polymers, impregnation of inorganic inert fillers, and addition of plasticizer. Among these methods, blending of polymer system has been found to be the most viable technique. Polymer blending not only improves the ionic conductivity but also exhibits good electrical and mechanical properties. Many polymer blend systems have been synthesized and investigated, such as poly(vinyl alcohol) (PVA)–poly (methyl methacrylate) (PMMA),[2] poly(vinyl acetate) (PVAc)–poly(vinylidene fluoride) (PVdF),[4] PVA–poly(styrene sulphonic acid) (PSA),[5] PVAc–PMMA,[6] poly(vinyl chloride) (PVC)–poly (ethyl methacrylate) (PEMA),[7,8] poly(ethylene oxide) (PEO)–PVdF,[9] PMMA–PVdF,[10,11] and PMMA–PVC.[12–17] In this study, blending of PMMA and PVC is used. The dipole–dipole interaction between hydrogen and chlorine atoms stiffens the polymer backbone. Hence, PVC acts as a mechanical stiffener in this polymer system.[18]

PMMA is selected because of its high surface resistance, good compatibility with most of the polymers, excellent interfacial stability toward the lithium electrodes, and high ability to solvate inorganic salts to form complexation between polymer and salt.[14,15] In contrast, PVC is chosen due to its good compatibility with the liquid electrolyte, high ability to form

Table I. Designations of Polymer Blend Electrolytes

Composition of (PMMA–PVC): LiTFSI	Designations
95 : 5	SPE 1
90 : 10	SPE 2
85 : 15	SPE 3
80 : 20	SPE 4
75 : 25	SPE 5
70 : 30	SPE 6
65 : 35	SPE 7
60 : 40	SPE 8
55 : 45	SPE 9
50 : 50	SPE 10

homogeneous hybrid film, and inexpensive as well as easy to solvate the inorganic salt because of its lone pair electrons at chlorine atom.[16,18] The same combination of PMMA–PVC polymer blend electrolytes was studied by Rajendran and Uma[16] with $LiBF_4$ as a salt and dibutyl phthalate (DBP) as plasticizer. In this study, lithium bis(trifluoromethanesulfonyl) imide (LiTFSI) is used as a doping salt because of its high delocalized electrons in $TFSI^-$ anion, which causes a low tendency for coordination with lithium cations.[19] Hence, lithium cations are more available for migration and this leads to an increase in ionic conductivity. The attempt of using LiTFSI is also because of its noncorrosive behavior toward electrodes.

In this work, impedance spectroscopy is used for different studies such as temperature dependence, conductivity measurement at ambient temperature, and dielectric study, which determines the relaxation process and electrode polarization effect in the polymer matrix. The main purpose of using this spectroscopy is to observe the participation of polymeric chain, segmental mobility of Li^+ ions, and generation process of mobile charge carriers in the polymer matrix by establishing ionic conduction mechanism.[2] In addition, horizontal attenuated total reflectance–Fourier transform infrared (HATR–FTIR) spectroscopy is performed to scrutinize the complexation between polymer and salt.

EXPERIMENTAL

Materials

PMMA with an average molecular weight of 350,000 g mol^{-1} (Aldrich), high-molecular-weight of PVC (Fluka), inorganic dopant salt, LiTFSI (Fluka), and solvent THF (J.T. Baker) were used without further purification in this study. The polymer blend electrolytes were prepared by solution-casting technique.

Preparation of Thin Films

Before the preparation of the polymer electrolytes, LiTFSI was dried at 100°C for 1 h to eliminate trace amounts of water. A fixed weight ratio of PMMA blended with PVC was used, that is, 70 : 30. The incorporation of LiTFSI was expressed as weight ratio. Appropriate amounts of PMMA, PVC, and LiTFSI were dissolved in THF, and the solution was continuously stirred for 24 h to obtain a homogenous mixture at room temperature. The solution was then cast on a glass Petri dish and allowed to evaporate slowly inside a fume hood. Free-standing thin film is eventually formed. Table I depicts the compositions and designations of the polymer blend electrolytes.

Characterizations

All the prepared samples were subjected to AC-impedance spectroscopy and HATR–FTIR. For impedance spectroscopy, the thicknesses of the thin films were measured by using micrometer screw gauge. The ionic conductivity of the samples was determined by using HIOKI 3532–50 LCR HiTESTER connected to a computer for data acquisition over a frequency range between 50 Hz and 1 MHz. The thin films were sandwiched between two stainless disc electrodes. HATR–FTIR analysis was performed by using FTIR Spectrometer Spectrum RX1 (Perkin-Elmer) with HATR, an internal reflection accessory, in the wave region between 4000 and 650 cm^{-1}. The resolution of the spectra was 4 cm^{-1} and recorded in the transmittance mode.

RESULTS AND DISCUSSION

AC-Impedance Studies

AC-impedance study is used to study the conductance properties of the polymer electrolytes. The bulk ionic conductivity of polymer electrolytes is determined by using the equation as shown below.

$$\sigma = \frac{\ell}{R_b A} \tag{1}$$

where ℓ is the thickness (cm), R_b is bulk resistance (Ω), and A is the known surface area (cm^2) of polymer electrolyte films. The semicircle fitting was accomplished to obtain R_b value. R_b of the thin electrolyte films is calculated from extrapolation of the semicircular region on Z' axis. The logarithm of ionic conductivity against various weight percentage of LiTFSI is demonstrated in Figure 1. On the basis of the obtained results, SPE 6 exhibits the highest ionic conductivity of $(1.111 \pm 0.09)\times10^{-6}$ S cm^{-1} at ambient temperature. When mass loading increases, the ionic conductivity also increases concurrently. The concentration of mobile charge carriers increases with the LiTFSI mass fraction and thus leads to improvement of ionic conductivity. In addition, the

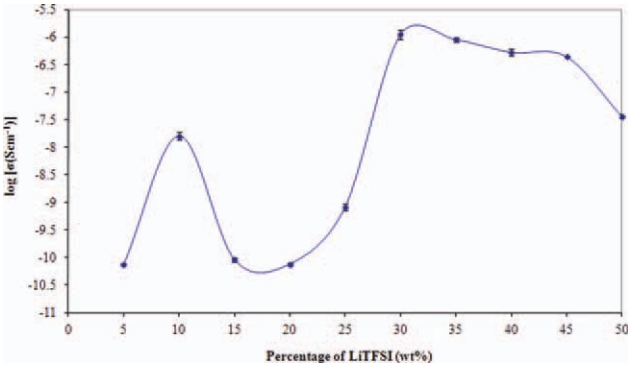

Figure 1. Variation of log ionic conductivity of PMMA–PVC–LiTFSI polymer electrolytes as a function of weight percentage LiTFSI at ambient temperature. [Color figure can be viewed in the online issue, which is available at wileyonlinelibrary.com.]

$TFSI^-$ ions tend to produce an electrostatic environment. Therefore, it decreases the mean hopping distance of charge carriers, which increases the ionic conductivity.[6] The inclusion of bulky anionic salt also reduces the glass transition temperature (T_g) of the polymer because of its plasticizing effect. The reduction of T_g softens the polymer backbone by weakening the interaction between the polymer matrix and lithium cations. As a result, it enhances the flexibility of polymer backbone, improves the ion migration within the polymer, and eventually increases the ionic conductivity.[20] However, on addition of 15 wt % of lithium salt, we found out that the ionic conductivity is decreased. It is suggestive of the repulsion force within the polymer matrix, and this restricts the mobility of polymer chain by adding LiTFSI further.[21] Moreover, the ion aggregation and ion pairing would block the ionic conducting pathway and diminish the effective number of charge carrier, impeding the ionic conductivity.

Beyond this weight percentage, the ionic conductivity increases with LiTFSI concentration again, to an optimum level. The increase in ionic conductivity is due to the long Coulombic forces range, which leads to redissociation of solvated ion pairs with increasing LiTFSI concentration. This contributes to increase in concentration of free mobile charge carriers, which are available for segmental migration. Hence, the ionic conductivity is increased as mobility and concentration of mobile charge carriers are increased. On addition of 30 wt % LiTFSI, the maximum ionic conductivity of $(1.111 \pm 0.09)\times10^{-6}$ S cm^{-1} is achieved. It implies the optimum limit of concentration and mobility of charge carriers. Furthermore, the optimum percolation threshold has been reached. This gives rise to the greatest extent of conductivity properties of lithium salt via formation of percolation pathways. The highest ionic conductivity is ultimately achieved. Above this optimum limit, the ionic conductivity is decreased. The retarding effect of ion cloud is more dominant rather than build-up of mobile charge carriers. This impedes the mobility of charge carriers in a rigid framework and induces a decrease in ionic conductivity.[16] The reduction of ionic conductivity is also assigned to salt precipitation, which leads to an increase in the viscosity of the ionic environment caused by ionic complex sites produced by the excess of Li^+.[20]

Figure 2 shows the typical Cole–Cole plots of complex impedance for SPE 6 in the temperature range of 298–353 K. Two well-defined regions, a slanted spike at low frequency and a semicircle at high frequency, are observed in low temperature range of 298–313 K. However, the semicircle disappears at high temperature. The semicircle portion reveals the characteristic of a parallel combination of bulk resistance and bulk capacitance of polymer matrix, as demonstrated in Figure 3(a). In other words, this conduction mechanism depends on the migration of Li^+ ion through the free volume of polymer matrix, which can be represented by a resistor at low frequency, whereas the polarization of immobile polymeric chain in the alternating field is represented by a capacitor at high frequency. A slanted spike is obtained instead of vertical spike, as exemplified in Figure 3(a,b). It indicates the nonideal mode of capacitance behavior in the polymer electrolytes and thus leads to the configuration of electrical double layer at electrolyte and electrode interface.

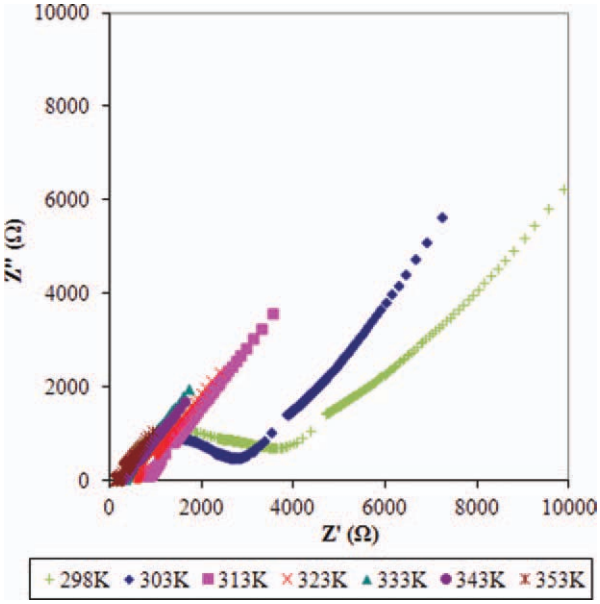

Figure 2. Complex impedance plot of SPE 6 in the temperature range 298–353 K. [Color figure can be viewed in the online issue, which is available at wileyonlinelibrary.com.]

This formation of constant phase element (CPE) implies the non-Debye properties of the polymer electrolytes. The inset of Figure 2(a) portrays the equivalent circuit of SPE 6 at ambient temperature. It is noteworthy that the slanted spike represents the CPE of the polymer, which indicates the polarization effect at the electrode–electrolyte boundary. Apart from that, the degree and slope of the inclination indicates the width of relaxation time distribution, whereas the charge carriers accumulate at the electrode and electrolyte interface before the electric field changes the direction.[21]

The disappearance of the semicircle in Figure 3(b) is due to the random dipole orientation in the side chains of polymer blend system and induces to a noncapacitance nature.[6] As aforementioned, the capacitance effect is characterized by polarization of immobile polymeric chain in the alternating current field. Therefore, only the resistive components in the polymer electrolytes prevail at this moment and then construct a local effective conducting pathway for ionic conduction of polymer electrolytes. As a result, the migration of ions is being enhanced as the electrical potential alternates between the positive and negative electrodes in the alternate current field. As a conclusion, the disappearance of semicircle region indicates that the current charge carriers are ions and results in an ion conduction mechanism.[2] Consequently, the capacitor is absent in the equivalent circuit, which has been depicted in inset of Figure 3(b). Besides, the resistor and CPE are connected in series path.

From Figure 2, the R_b decreases as the temperature increases. As a result, ionic conductivity increases with temperature. It is ascribed to the enhancement of thermal mobility of polymer chain in the polymer electrolyte system and rate of dissociation of LiTFSI as temperature increases. The explanation is further discussed in the temperature dependence–ionic conductivity study.

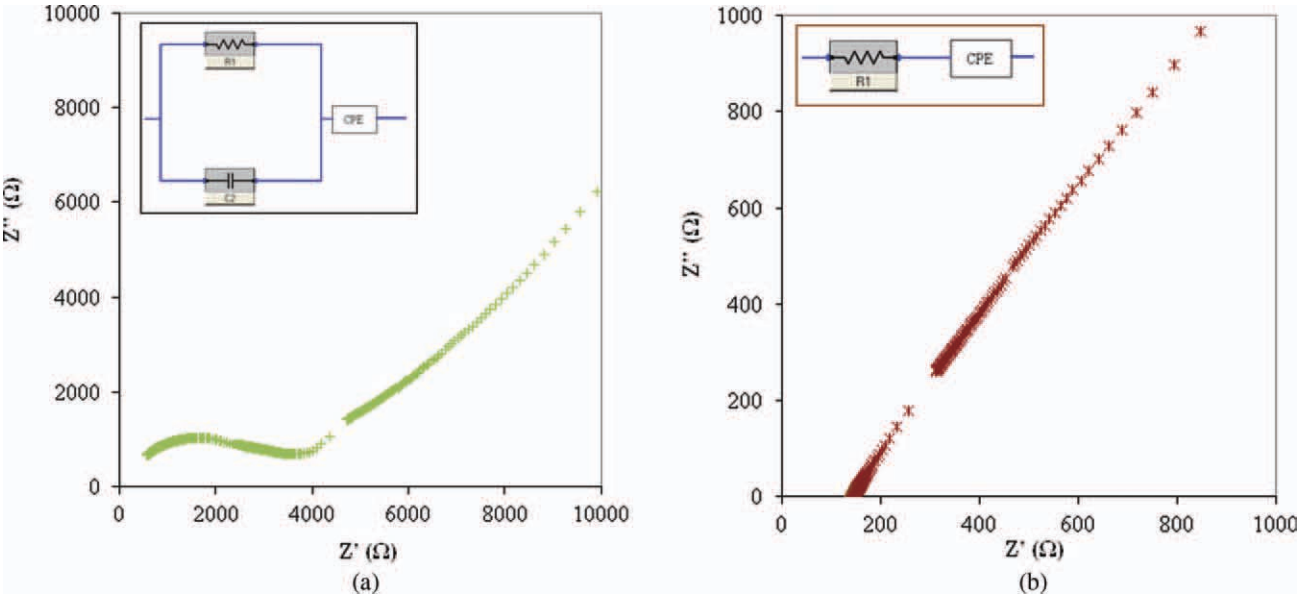

Figure 3. (a) Typical Cole–Cole plot of complex impedance for SPE 6 and its equivalent circuit (inset figure) at ambient temperature. (b) Typical Cole–Cole plot of complex impedance for SPE 6 and its equivalent circuit (inset figure) at 353K. [Color figure can be viewed in the online issue, which is available at wileyonlinelibrary.com.]

Temperature Dependence–Ionic Conductivity Studies

Figure 4 illustrates the ionic conductivity of SPEs 3, 6, and 8 against the reciprocal absolute temperature. According to this figure, it is further proven that ionic conductivity increases with a function of temperature. As temperature increases, it causes the expansion of polymer matrix and thus weakens the interaction within the polymer matrix. This initiates the decoupling of Li cations from the polymer matrix. Besides, as the temperature is increased, the polymeric chain acquires faster internal modes and thus promotes the bond rotation, resulting in faster segmental mobility. Consequently, the intrachain and interchain of ion hopping mechanisms are favorable, which in turn result in higher ionic conductivity.[6] Furthermore, it divulges that the polymer electrolyte is in completely glassy phase as there is no abrupt jump in the variation of ionic conductivity with respect to temperature.[22] Because the regression values are close to unity, it implies that the variation in ionic conductivity with temperature obeys the linear relationship, which is Arrhenius relationship:

$$\sigma = A \exp\left(\frac{-E_a}{kT}\right) \tag{2}$$

where A is a constant, which is proportional to the amount of charge carriers, E_a is activation energy, k is Boltzmann constant, that is, 8.6173×10^{-5} eV K^{-1}, and T represents the absolute temperature in K. The values of constant A are 0.0048, 36.36, and 15.27 S cm^{-1} for SPEs 3, 6, and 8, respectively. In this theory, the hopping mechanism is favorable. For Arrhenius relationship, it states that the nature of transportation of charge carrier is similar with the migration in ionic crystal. The charge carriers are decoupled from the segmental motion in polymer chain as the interaction of polar group of the blended polymers with Li cations is weaker. Thus, it creates vacant sites or empty voids in the polymer chain. Therefore, the ions tend to occupy these neighboring vacant sites. This transportation of charge carriers increases the ionic conductivity.

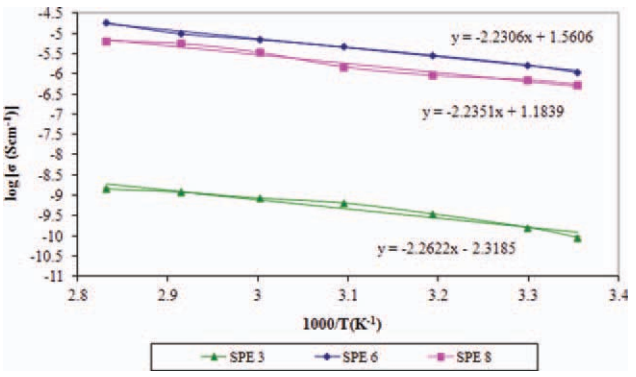

Figure 4. Arrhenius plot of ionic conductivity of SPEs 3, 6, and 8. [Color figure can be viewed in the online issue, which is available at wileyonlinelibrary.com.]

From the derivation of equation mentioned earlier in the text, the activation energy (E_a), which is a combination of energy required for defect migration of charge carriers and defect formation is determined. It is evaluated from the slope of the Arrhenius plot. The E_a values obtained for SPEs 3, 6, and 8 are 0.4489 eV, 0.4427 eV, and 0.4436 eV, respectively. As can be seen in eq. (2), the ionic conductivity is inversely proportional to E_a. The theory can be proven in this study. As expected, SPE 8 has higher E_a value than SPE 6. It is due to the salt precipitation as a result of high LiTFSI mass fraction.

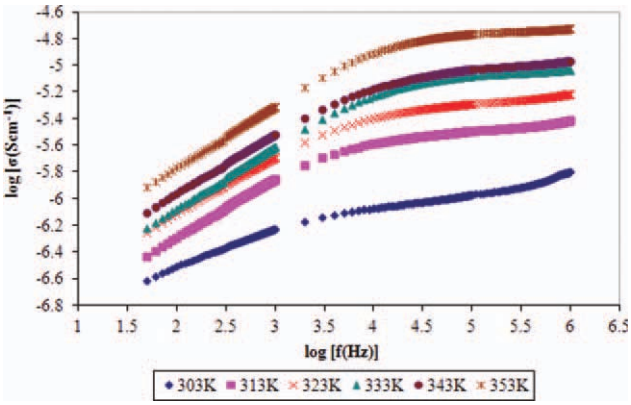

Figure 5. Frequency-dependent conductivity for SPE 6 in the temperature range of 303–353 K. [Color figure can be viewed in the online issue, which is available at wileyonlinelibrary.com.]

Conductivity-Frequency Dependence

To understand the relaxation process of polymer electrolyte, the ionic conductivity of polymer electrolytes with respect to frequency is investigated. In this study, the conductivity is expressed as below:

$$\sigma = \frac{G\ell}{A} \tag{3}$$

where G is the conductance. Figure 4 depicts the frequency-dependence conductivity for SPE 6 at different temperatures. The sample exhibits frequency-dependence behavior within the frequency range. As shown in Figure 4, the ionic conductivity increases with frequency and temperature. The low conductivity in the low frequency dispersion region is attributed to the space charge polarization effect at the electrode–electrolyte interface, indicating the non-Debye characteristic of polymer matrix.[23] It may be due to the enhancement of space charge carriers accumulated at this interface and thus the effectiveness of applied field across the sample is decreased. Thus, the density of mobile ions available for migration is greatly reduced, which is in accordance with a decrease in ionic conductivity.[6] In contrast, the concentration of space charge, which builds up at the electrode–electrolyte interface is lesser at high frequency and leads to an increase in mobility of charge carriers. Hence, the ionic conductivity increases with frequency.

Similarly, the ionic conductivity increases with temperature. As temperature increases, the hopping process of charge carriers is more favored and leads to an increase in movement of ions and eventually to an increment in ionic conductivity. It also indicates the presence of hopping mechanisms between coordinating sites, local structural relaxations, and segmental migration of the polymer matrix.[3]

Dielectric Behavior Studies

Dielectric relaxation study is an approach to investigate the relaxation behavior and polarization effect onto the polymer electrolytes. The complex dielectric behavior of a polymer system is expressed as:

$$\varepsilon^* = \varepsilon' - i\varepsilon'' \tag{4}$$

where ε' and ε'' are real and imaginary parts of dielectric constant of the polymer electrolyte system. On the contrary, these real and imaginary parts of the dielectric constants are determined as follows:

$$\varepsilon' = \frac{C_p\ell}{\varepsilon_o A} \tag{5}$$

$$\varepsilon'' = \frac{\sigma}{\omega\varepsilon_o} \tag{6}$$

where C_p is parallel capacitance, ε_o is permittivity in free space (also known as electric constant), and ω is angular frequency. The real part of dielectric relaxation constant (also known as dielectric constant) is the direct measure of stored charge,[5] whereas imaginary permittivity of the dielectric relaxation constant (also known as dielectric loss) is a direct measure of dissipation of energy, which results of transportation of charge carriers and polarization effect of charge carriers.[12] Figure 6(a,b) illustrate the frequency-dependence variation of real (ε') and imaginary (ε'') permittivity of the

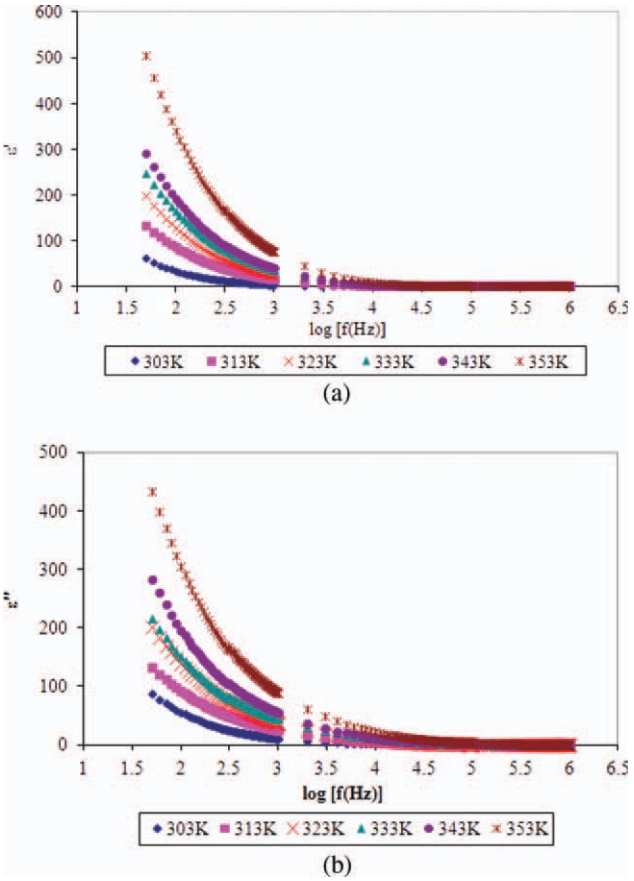

Figure 6. (a) Typical plot of the variation of real part of dielectric constant (ε') with frequency for SPE 6 in the temperature range of 303–353 K. (b) Typical plot of the variation of imaginary part of dielectric constant (ε'') with frequency for SPE 6 in the temperature range of 303–353 K. [Color figure can be viewed in the online issue, which is available at wileyonlinelibrary.com.]

dielectric relaxation constant for SPE 6 in the temperature range of 303–353 K, respectively. Both dielectric constant and dielectric loss rise sharply toward low frequency. This observed variation in ε' and ε'' as a function of frequency is attributed to accumulation of charge at the electrode and electrolyte interface and yields a space charge region. With the presence of this polarization effect, it reveals the non-Debye type of behavior.

In contrast, ε' and ε'' decrease with increasing frequency. It is attributed to high reversal of the external electric field at the electrode and electrolyte interface. Subsequently, it causes a reduction in density of charge carriers at this interface and reduces the diffusion of excessive ions in the direction of electric field, inducing to the inhibition of orientation of dipoles. This leads to a decrease in polarization and then weakens the interaction of dipoles and electric field. As a consequence, ε' and ε'' decrease as frequency increases.[5,22] On the contrary, ε' and ε'' increase with temperature. It is due to the high bond rotation of interactive bonds within the polymer matrix and hence enhances the extent of lithium salt dissociation and rate of redissociation of ion aggregates. This contributes to an increment of density of mobile charge carriers, which are favourable for transportation.[5] As shown in these figures, the dielectric constants at 353 K shown the highest value in the interval of 303–353 K and this divulges that the ionic conductivity at 353 K is the optimum value. It has been proven in the Cole–Cole plots and temperature-dependence studies. The absence of polarization peaks in these figures may be attributed to the phase-separated morphology of the polymer electrolytes.[11]

Dielectric Moduli Formalism

The dielectric moduli analysis is a further study to investigate the dielectric properties of polymers and their blends by suppressing the polarization effects of the electrode and thus get rid of interfacial effect.[11] The complex dielectric modulus can be determined by the equation below:

$$M^* = M' + iM'' \tag{7}$$

where M' is the real part of dielectric modulus and M'' is the imaginary part of dielectric modulus. The real and imaginary parts of dielectric moduli are expressed as below:

$$M' = \frac{\varepsilon'}{[(\varepsilon')^2 + (\varepsilon'')^2]} \tag{8}$$

$$M'' = \frac{\varepsilon''}{[(\varepsilon')^2 + (\varepsilon'')^2]} \tag{9}$$

The real (M') and imaginary (M'') parts of dielectric moduli as a function of frequency for SPE 6 in the temperature range of 303–353 K are exemplified in Figure 7(a,b), respectively. At low frequency regime, both M' and M'' tend to approach zero as shown in these figures. This reveals the insignificance of polarization effect at the electrode and electrolyte interface at low frequency range. A long tail is observed at low frequency regime in these figures. It implies that the capacitance associated with electrodes is higher.[23] Even though well-defined dispersion peaks

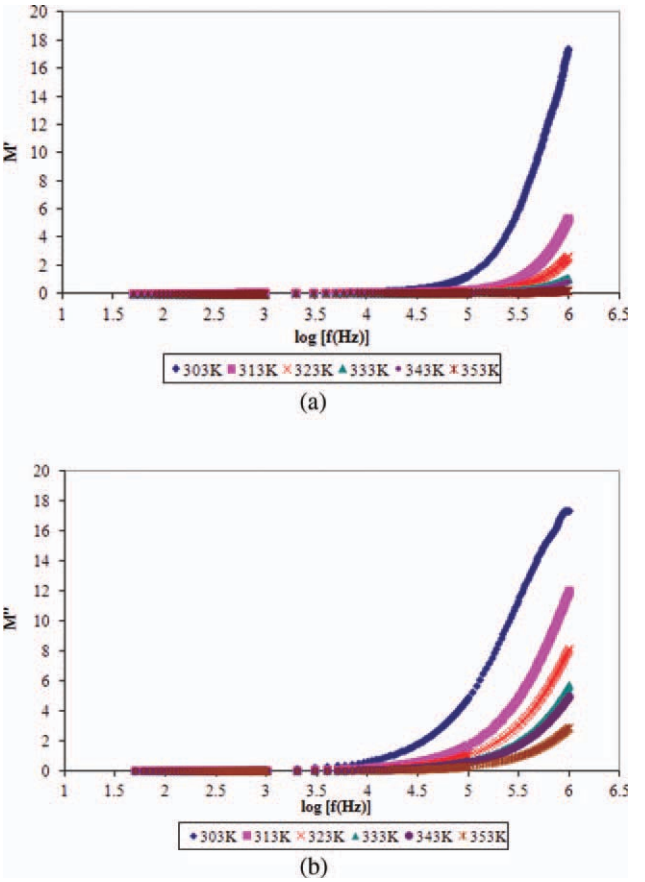

Figure 7. (a) Variation of real modulus (M') as a function of frequency for SPE 6 in the temperature range of 303–353 K. (b) Variation of imaginary modulus (M'') as a function of frequency for SPE 6 in the temperature range of 303–353 K. [Color figure can be viewed in the online issue, which is available at wileyonlinelibrary.com.]

are not observed in both of these variations, M' and M'' show an obvious increase at high frequency regime. The curve peaks indicate the presence of bulk effect in the polymer matrix and hence imply that polymer electrolytes are ionic conductors. The intensity of these peaks decreases with increasing temperature. It may be due to the plurality of relaxation mechanism where the time is required to accumulate charge carriers at the electrode and electrolyte interface before the field changes the direction.[22]

HATR–FTIR Studies

Table II shows the designations of the characteristic peaks of PMMA, PVC, and LiTFSI for SPE 6. The HATR–FTIR spectra for pure PMMA, pure PVC, PMMA–PVC, pure LiTFSI, and SPE 6 are shown in Figure 8. All the characteristic peaks of PMMA and PVC are present in PMMA–PVC spectra. From this figure, there are five new peaks appearing. These new peaks are assigned as overlapping of symmetric bending mode of CF_3 and combination of C—S and S—N stretching mode of LiTFSI, overlapping of asymmetric S—N—S stretching, and S=O bonding mode of LiTFSI, C—SO_2—N bonding mode of LiTFSI, C—SO_2—N bonding mode of LiTFSI and combination of asymmetric SO_2 stretching and C—SO_2—N bonding mode of LiTFSI

Table II. Assignments of Vibrational Modes of PMMA, PVC, and LiTFSI for SPE 6 Polymer Matrix System

Description vibration modes	Wavenumber (cm^{-1})	References
Cis C—H wagging mode of PVC	708	13
Overlapping of symmetric bending mode of CF_3, δ_s (CF_3), and combination of C—S and S—N stretching of LiTFSI	746	12,16
C—Cl stretching of PVC	847	13
C—O vibrational mode of C—O—C bond of PMMA	963	15
Trans C—H wagging mode of PVC	981	13
Overlapping of asymmetric S—N—S stretching and S=O bonding mode of LiTFSI	1056	14,16
C—SO_2—N bonding mode of LiTFSI	1133	12
Overlapping of symmetric stretching mode of CF_3, ν_{as} (CF_3) of LiTFSI and asymmetric O—CH_3 stretching mode of PMMA	1186	12,13
C—H rocking mode of PVC	1232	13
C—SO_2—N bonding mode of LiTFSI	1327	13,16,17
Combination of asymmetric SO_2 stretching and C—SO_2—N bonding mode of LiTFSI	1349	17,24
O—CH_3 asymmetric bending mode of PMMA	1444	24
C=O stretching mode of PMMA	1711	24
Overlapping of C—H stretching mode of PMMA, C—H stretching mode PVC and S—CH_3 bonding mode of LiTFSI	2992-2850	13,15,16

at 746, 1056, 1133, 1327, and 1349 cm^{-1}, respectively. It indicates that there is an establishment for formation of polymer salt system. In addition, there is an obvious change in shape for the S—CH_3 bonding mode of LiTFSI in the region of 2979–2876 cm^{-1}. In the pure LiTFSI spectra, it appears as two sharp peaks, which become a single peak with two small shoulders on incorporation of PMMA–PVC polymer blend matrix, as shown in Figure 9. This is due to overlapping of C—H stretching mode of PMMA, C—H stretching mode of PVC, and S—CH_3 bonding mode of LiTFSI. It reveals that there is a binding of PMMA, PVC, and LiTFSI. Furthermore, a distinctive change of characteristic absorption in the region of 1186–1133 cm^{-1} is illustrated in Figure 10. A single peak with a small shoulder has been changed to double peaks. In this region, 1133 cm^{-1} is

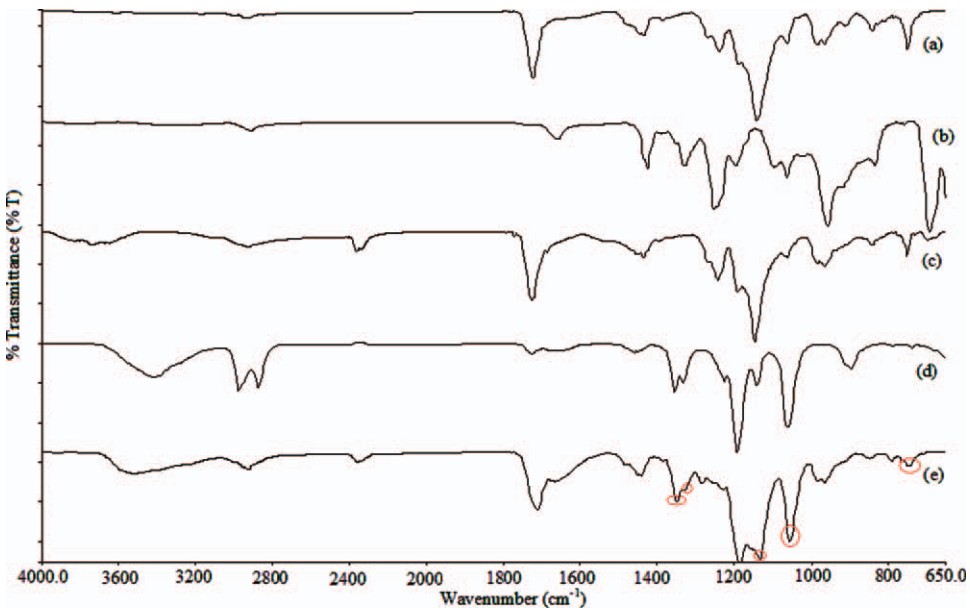

Figure 8. HATR–FTIR spectra for (a) pure PMMA, (b) pure PVC, (c) PMMA–PVC, (d) LiTFSI, and (e) SPE 6. [Color figure can be viewed in the online issue, which is available at wileyonlinelibrary.com.]

assigned as C—SO_2—N bonding mode of LiTFSI, whereas 1186 cm^{-1} is assigned as overlapping of symmetric stretching mode of CF_3 of LiTFSI and asymmetric O—CH_3 stretching mode of PMMA. This discloses the interaction between PMMA and LiTFSI.

Moreover, the characteristic peaks of cis C—H wagging mode of PVC, C—Cl stretching of PVC, C—O vibrational mode of C—O—C bond of PMMA, and trans C—H wagging mode of PVC are shifted from 693, 837, 966, and 986 cm^{-1} to 708, 847, 963, and 981 cm^{-1}, respectively. It divulges that there is an interaction between PMMA, PVC, and LiTFSI. Apart from that, the intensity of characteristic absorption peaks has also been changed. As exemplified in Figure 10, there is an observable change in intensity of C=O stretching mode of PMMA at 1711 cm^{-1}. Intensity of this sharp peak increases by 1.35% in transmittance mode from 1.90 to 3.25%. Moreover, it undergoes shifting in wavenumber that is shifted from 1725 cm^{-1}. This might be due to an interaction of C=O of ester in PMMA with LiTFSI via coordination bond. Similarly, the intensity of O—CH_3 asymmetric bending mode of PMMA at 1444 cm^{-1} is also enhanced by 0.54% on addition of LiTFSI. It changes from 0.6 to 1.14%, whereby it changes from 1434 to 1444 cm^{-1} in terms of shift in peak. This may be attributed to the occurrence of an interaction of CH_3 in PMMA and CF_3 in LiTFSI via coordination bond involving hydrogen bond of hydrogen atom of

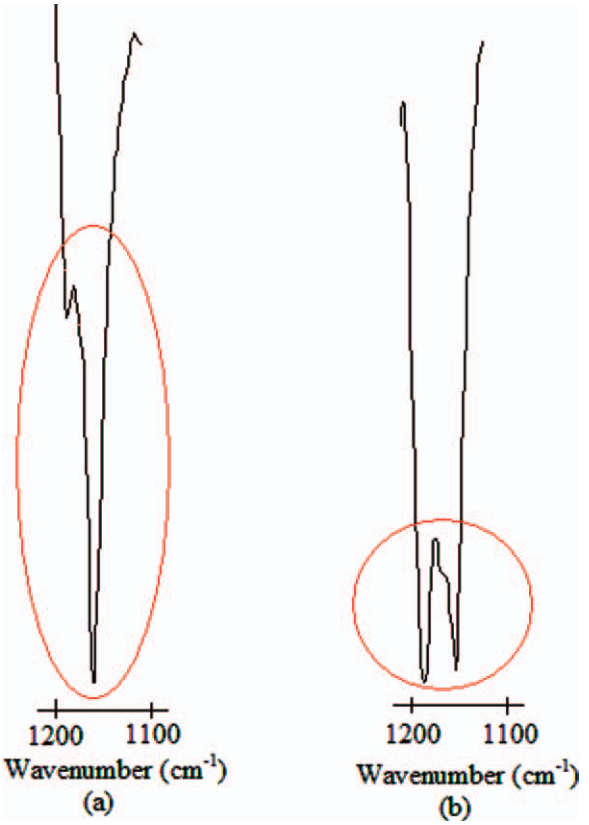

Figure 9. The comparison of change in shape of overlapping asymmetric O—CH_3 stretching mode of PMMA and symmetric stretching mode of CF_3 of LiTFSI in (a) PMMA–PVC and (b) SPE 6. [Color figure can be viewed in the online issue, which is available at wileyonlinelibrary.com.]

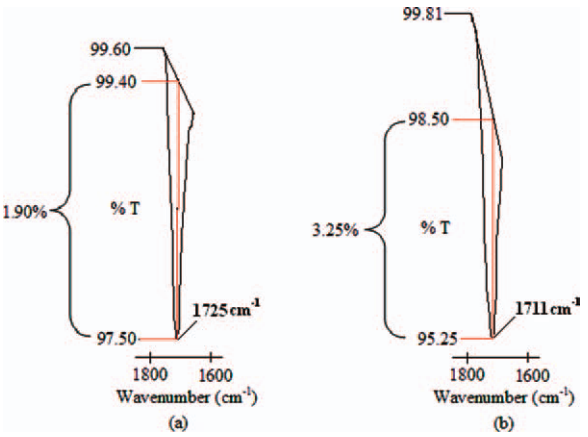

Figure 10. The comparison of change in intensity of C=O stretching mode of PMMA in (a) PMMA–PVC and (b) SPE 6. [Color figure can be viewed in the online issue, which is available at wileyonlinelibrary.com.]

PMMA with fluorine atom of LiTFSI leading to a complexation between PMMA and LiTFSI. On the contrary, the intensity of C—H rocking mode of PVC is reduced by 0.80%, which is from 1.20% in PMMA–PVC spectra, and this peak is shifted from 1242 to 1232 cm^{-1}. This also implies that there is a formation of hydrogen bonding of hydrogen atom of PVC with fluorine atom of LiTFSI and this initiates coordination between PVC and LiTFSI. On the basis of these results, the presence of complexation between PMMA, PVC, and LiTFSI can be established.

CONCLUSION

In this work, the highest ionic conductivity of $(1.111 \pm 0.09) \times 10^{-6}$ S cm^{-1} was achieved on addition of 30 wt % of LiTFSI salt. The temperature dependence–ionic conductivity study obeys Arrhenius rules. This law suggests the occurrence of ionic hopping mechanism in the polymer matrix. In dielectric relaxation study, the polarization effect is the main contributor to increase these ε' and ε'' values at low frequency region. Only bulk effect can be observed in the variation of M' and M'' at high frequency regime. The AC-impedance and dielectric study reveal the occurrence of non-Debye characteristic of polymer electrolytes. On the basis of HATR–FTIR analysis, there is a complexation between PMMA, PVC, and LiTFSI with the presence of new peaks, change in shift, change in intensity, and change in shape.

ACKNOWLEDGMENTS

This work was supported by the Fundamental Research Grant Scheme (FRGS), Malaysia. Chiam-Wen Liew gratefully acknowledges the "Skim Bright Sparks Universiti Malaya" (SBSUM) for financial support.

REFERENCES

1. Gray, F. M.; Corron, J. A. In Polymer Electrolyte; The Royal Society of Chemistry: Cambridge, **1997.**
2. Rajendran, S.; Sivakumar, M.; Subadevi, R. *Mater. Lett.* **2004,** *58*, 641.

3. Ramesh, S.; Winie, T.; Arof, A. K. *Eur. Polym. J.* **2007,** *43*, 1963.
4. Baskaran, R.; Selvasekarapandian, S.; Kuwata, N.; Kawamura, J.; Hattori, T. *Mater. Chem. Phys.* **2006,** *98*, 55.
5. Kumar, M. S.; Bhat, D. K. *Phys. B* **2009,** *404*, 1143.
6. Baskaran, R.; Selvasekarapandian, S.; Kuwata, N.; Kawamura, J.; Hattori, T. *Solid State Ionics* **2006,** *177*, 2679.
7. Rajendran, S.; Prabhu, M. R.; Rani, M. U. *J. Power Sources* **2008,** *180*, 880.
8. Han, H. S.; Kang, H. R.; Kim, S. W.; Kim, H. T. *J. Power Sources* **2002,** *112*, 461.
9. Yang, Y.; Zhou, C. H.; Xu, S.; Hu, H.; Chen, B.L.; Zhang, J.; Wu, S. J.; Liu, W.; Zhao, X. Z. *J. Power Source* **2008,** *185*, 1492.
10. Nicotera, I.; Coppola, L.; Oliviero, C.; Castriota, M.; Cazzanelli, E. *Solid State Ionics* **2006,** *177*, 581.
11. Cui, Z. Y.; Xu, Y. Y.; Zhu, L. P.; Wei, X. Z.; Zhang, C. F.; Zhu, B. K. *Matter. Lett.* **2008,** *62*, 3809.
12. Stephan, A. M.; Renganathan, N. G.; Kumar, T. P.; Thirunakaran, R.; Pitchumani, S.; Shrisudersan, J.; Muniyandi, N. *Solid State Ionics* **2000,** *130*, 123.
13. Rajendran, S.; Uma, T.; Mahalingam, T. *Eur. Polym. J.* **2000,** *36*, 2617.
14. Choi, N. S.; Park, J. K. *Electrochim. Acta.* **2001,** *46*, 1453.
15. Stephan, A. M.; Saito, Y.; Muniyandi, N.; Renganathan, N. G.; Kalyanasundaram, S.; Elizabeth, R. N. *Solid State Ionics* **2002,** *148*, 467.
16. Rajendran, S.; Uma T. *J. Power Sources* **2000,** *88*, 282.
17. Li, W.; Yuan, M.; Yang, M. *Eur. Polym. J.* **2006,** *42*, 1396.
18. Ramesh, S.; Chai, M. F. *Mater. Sci. Eng. B* **2007,** *139*, 240.
19. Ramesh, S.; Ng, K. Y. *Curr. Appl. Phys.* **2009,** *9*, 329.
20. Baskaran, R.; Selvasekarapandian, S.; Kuwata, N.; Kawamura, J.; Hattori, T. *J. Phys. Chem. Solids* **2007,** *68*, 407.
21. Marcondes, R. F. M. S.; D'Agostini, P. S.; Ferreira, J.; Girotto, E. M.; Pawlicka, A.; Dragunski, D. C. *Solid State Ionics* **2010,** *181*, 586.
22. Venkateswarlu, M.; Reddy, K. N.; Rambabu, B.; Satyanarayana, N. *Solid State Ionics* **2000,** *127*, 177.
23. Ramesh, S.; Arof, A. K. *Mater. Sci. Eng. B* **2001,** *85*, 11.
24. Fernandez, M. E.; Diosa, J. E.; Vargas, R. A. *Microelectronics J* **2008,** *39*, 1344.